Korean J. Chem. Eng., 32(6), 1075-1080 (2015)
DOI: 10.1007/s11814-014-0287-9

pISSN: 0256-1115
eISSN: 1975-7220

Effect of Pt coverage in Pt-deposited Pd nanostructure electrodes on electrochemical properties

Ah-Reum Park, Young-Woo Lee, Da-Hee Kwak, and Kyung-Won Park†

Department of Chemical Engineering, Soongsil University, Seoul 156-743, Korea
(*Received 7 May 2014 • accepted 24 September 2014*)

Abstract−We have fabricated Pt-deposited Pd electrodes via a two-gun sputtering deposition system by separately operating Pd and Pt target as a function of sputtering time of Pt target. For Pt-deposited Pd electrodes (Pd/Pt-X), Pd were first deposited on the substrates at 20 W for 5 min, followed by depositing Pt on the Pd-only electrodes as a function of sputtering time (X=1, 3, 5, 7, and 10 min) at 20 W on the Pt target. As the sputtering time of Pt target increased, the portion of Pt on the Pd electrodes increased, representing an increased coverage of Pt on the Pd electrodes. The Pd/Pt-7 electrode having an optimized Pt coverage exhibits an excellent electrocatalytic activity for methanol oxidation reaction.

Keywords: Sputtering Deposition System, Pt Coverage, Pd Electrode, Methanol Oxidation Reaction, Electrochemistry

INTRODUCTION

Direct methanol fuel cells (DMFCs) are considerably attractive electrochemical power sources with low operating temperatures and high energy density of methanol as a fuel. The excellent electrocatalytic activity of Pt for methanol electrooxidation at low temperatures makes this metal electrocatalyst extremely suitable for use as an anode in DMFCs. However, since pure Pt is readily poisoned by intermediates produced during methanol electrooxidation, Pt-M (M=Ru, Os, Ir, and Pd) alloy catalysts need to be synthesized to overcome the poisoning effect of Pt catalyst. In general, the CO-poisoned Pt can be regenerated via the reaction of surface CO with oxygen species associated with elements such as Ru and Os to yield CO_2. In heterogeneous catalysis, bimetallic catalysts, which often show electronic and chemical properties that are distinct from those of their parent metals, offer the opportunity to obtain new catalysts with improved activity and stability. In particular, since Pt-Pd based nanostructure catalysts exhibit highly active oxygen reduction reaction and methanol oxidation reaction, Pt-Pd nanocatalysts could be considered as an alternative of Pt-Ru alloy catalysts for low temperature DMFC [1-5].

To understand the origins of the novel catalytic properties, bimetallic surfaces have also gained a considerable interest for fundamental surface science research. It is well-known that bimetallic surfaces often can show particular properties that are not present on either of the parent metal surfaces. In the preparation method for the bimetallic surface electrodes in an electrocatalysis study, sputtering deposition method could provide various useful electrodes such as alloy, island, or layered structures [6-8]. Hwang et al. prepared Pt-based alloy electrocatalysts with early transition metals for oxygen reduction reaction using high-pressure co-sputtering to investigate the relationship between electronic structure modification and stability [9]. We investigated the effect of Ru states on catalytic activity of Pt, Pt on Ru thin-film electrodes with various (electro) chemical states designed by means of sputtering method [10]. Furthermore, to identify the effect of composition in the PtRu electrocatalysts on catalytic activity, PtRu electrodes were fabricated by co-sputtering deposition method as a function of sputtering time of Pt and Ru targets [11]. Here, to investigate electrocatalytic activity of Pt layers on Pd electrodes, we fabricated Pd/Pt electrodes with a variety of coverage via a two-step sputtering deposition process. The structural and electrochemical properties of the Pd/Pt electrodes were characterized by transmission electron microscopy (TEM), energy dispersive X-ray spectroscopy (EDS), and cyclic voltammetry.

EXPERIMENTAL

1. Sample Preparation

To estimate electrochemical properties of Pt-deposited Pd (Pd/Pt) electrodes for methanol electrooxidation, the Pd/Pt electrodes were fabricated by two-step sputtering process with Pt and Pd targets. Indium tin oxide (ITO) coated glass electrodes and Cu grids were used as the substrates for electrochemical and TEM analysis, respectively. Pd metal and Pt metal were used as the target materials. The base pressure was less than 5×10^{-6} torr and the working pressure was 1.1×10^{-2} torr. The sputtering was performed under an atmosphere of inert Ar gas at 30 SCCM at room temperature. The Pd electrodes were deposited for 5 min at 20 W on the Pd target (denoted as Pd-only). For Pt-deposited Pd electrodes (Pd/Pt-X), Pd were first deposited on the substrates for 5 min at 20 W, followed by depositing Pt on the Pd-only electrodes as a function of sputtering time (X=1, 3, 5, 7, and 10 min) at RF powers of 20 W on the Pt target (denoted as Pd/Pt-1, Pd/Pt-3, Pd/Pt-5, Pd/Pt-7,

†To whom correspondence should be addressed.
E-mail: kwpark@ssu.ac.kr, snow7292@naver.com

and Pd/Pt-10), respectively.

2. Structural and Electrochemical Analysis

The size, morphology, and composition of the electrodes were analyzed by TEM using an FEI Tecnai F30 system operated at 300 kV and EDS combined with the TEM analysis. The electrochemical properties were measured in a three-electrode cell using a potentiostat (Eco Chemie, AUTOLAB) at room temperature with a scan rate of 50 mV s^{-1}. Pt wire and Ag/AgCl (in saturated 3 M KCl) were used as a counter and reference electrode, respectively. The ITO electrodes deposited were used as a working electrode. Cyclic voltammograms (CVs) of the Pt-covered Pd electrodes were obtained in Ar-saturated 0.1 M $HClO_4$ and 0.1 M $HClO_4$+2.0 M CH_3OH with a scan rate of 50 mV s^{-1} at room temperature.

RESULTS AND DISCUSSION

Fig. 1 shows a schematic illustration of Pt-deposited Pd electrodes fabricated via a two-step sputtering deposition process by separately operating Pd and Pt targets as a function of sputtering time of Pt target. First, Pd nanophases are deposited on the ITO electrodes by sputtering Pd target for 5 min in Ar atmosphere. After the formation of Pd nanophase electrodes, the Pt layers on the Pd electrodes are formed by alternately operating Pt target for different sputtering times (Pd/Pt-X, X=1, 3, 5, 7, and 10 min).

Fig. 2 shows TEM images and size histograms of Pt-deposited Pd electrodes fabricated as a function of sputtering time of Pt target in the sputtering system. The nanophase sizes of Pd-only, Pd/Pt-1, Pd/Pt-3, Pd/Pt-5, Pd/Pt-7, and Pd/Pt-10 are 6.06, 7.27, 8.08, 9.07, 10.06, and 11.44 nm, respectively, representing the increased size of Pd/Pt nanophases with increasing sputtering deposition

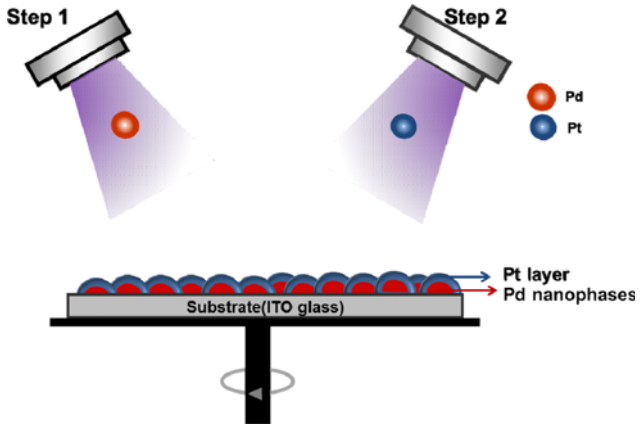

Fig. 1. Schematic illustration of a two-gun sputtering deposition system for Pt-deposited Pd electrodes (Pd/Pt-X) fabricated by separately operating Pd and Pt targets as a function of sputtering time (X=1, 3, 5, 7, and 10 min) of Pt target.

time (size histograms of Fig. 2). The insets of Fig. 2 show high-resolution TEM images of the Pd/Pt electrodes. The d-spacing of 2.241 Å in the Pd-only corresponds to {111} facets of Pd face-centered cubic (fcc) structure (Fig. 2(a)). As the sputtering time of Pt target increases, the d-spacings corresponding to {111} facets of Pd and Pt coexist. The Pd/Pt-10 exhibits the dominant d-spacing (2.262 Å) corresponding to {111} facets of Pt, indicating an increased coverage of Pt layers on the Pd electrodes.

Elemental mapping images and EDS spectra of the sputtered Pd/Pt electrodes were characterized as indicated in Fig. 3. The elemental mapping profiles show that the homogeneous distribution

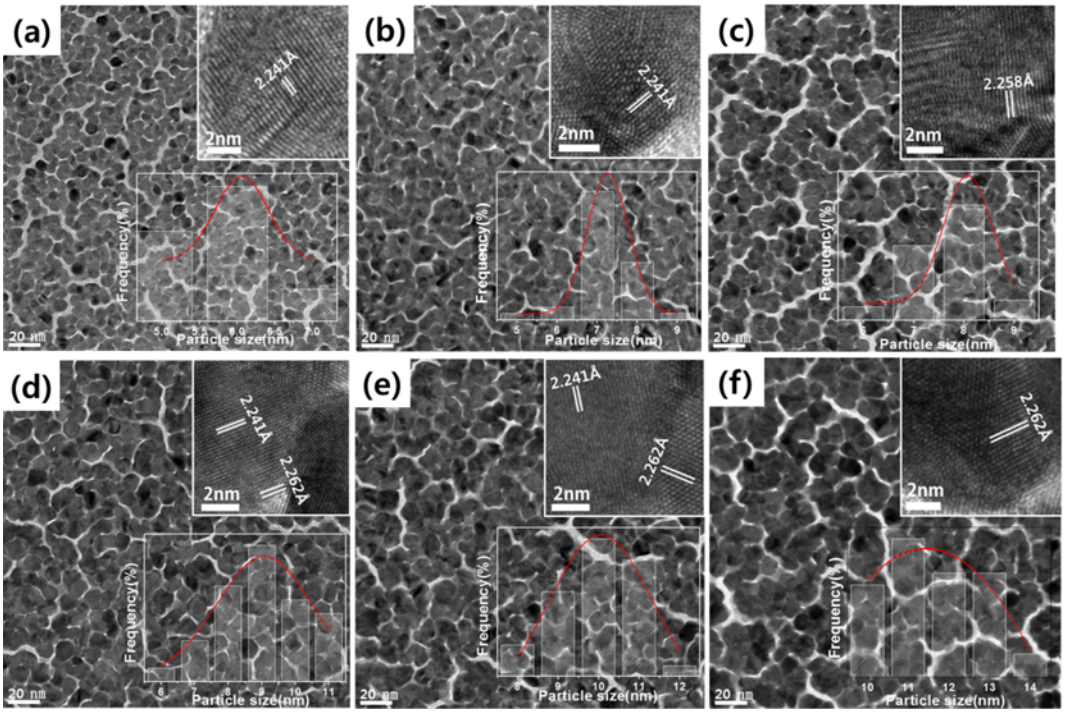

Fig. 2. TEM images of Pt-deposited Pd electrodes fabricated by the sputtering system: (a) Pd-only, (b) Pd/Pt-1, (c) Pd/Pt-3, (d) Pd/Pt-5, (e) Pd/Pt-7, and (f) Pd/Pt-10.

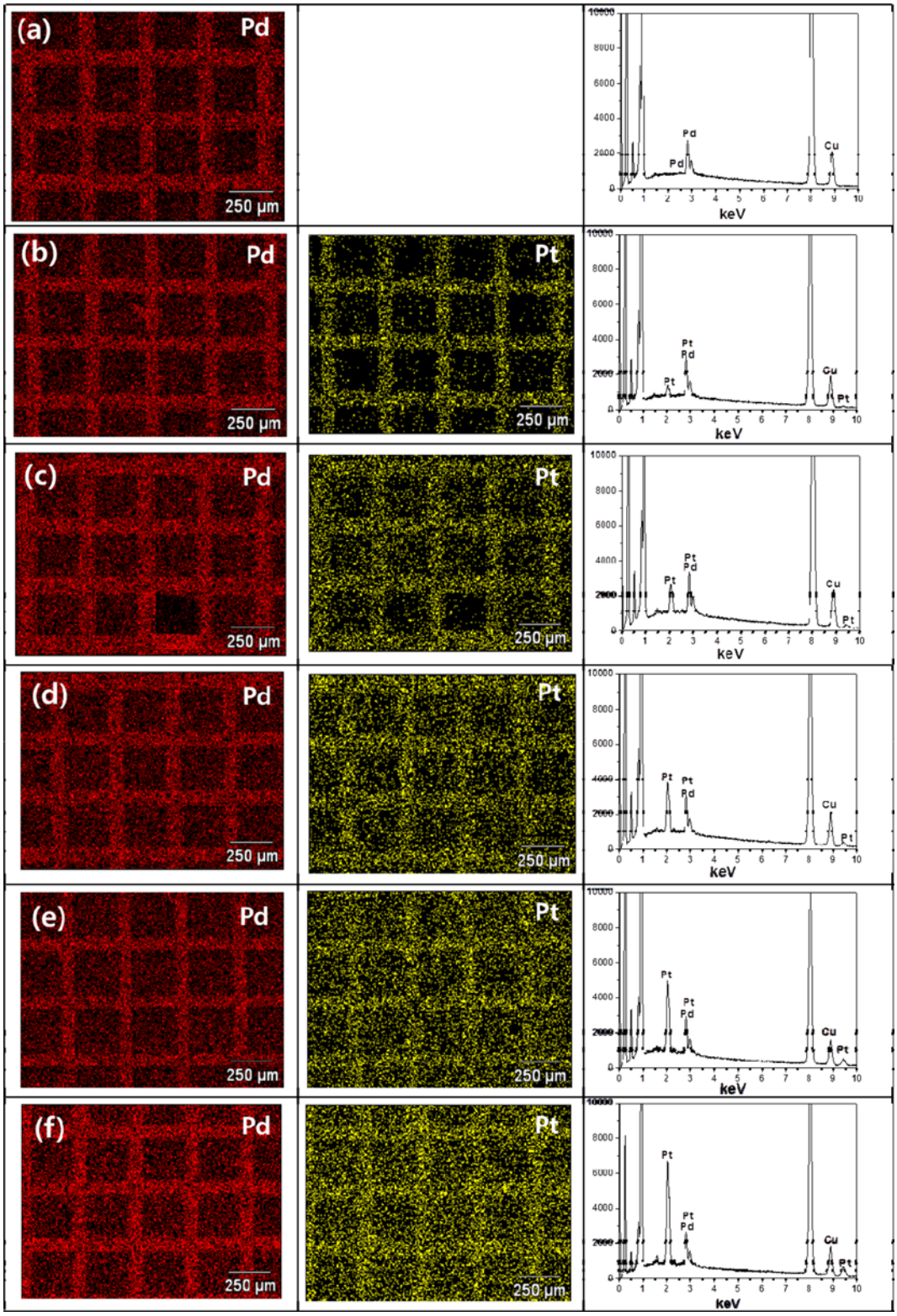

Fig. 3. Elemental distributions of Pd (red) and Pt (green) and EDX spectra of the sputtered electrodes: (a) Pd-only, (b) Pd/Pt-1, (c) Pd/Pt-3, (d) Pd/Pt-5, (e) Pd/Pt-7, and (f) Pd/Pt-10.

of Pt gradually increases in contrast to that of Pd, representing an increased coverage of Pt layers on Pd electrodes with increasing sputtering deposition time of Pt target. The peak intensity ratios of Pd to Pt measured by EDS spectra for Pd/Pt-1, Pd/Pt-3, Pd/Pt-5, Pd/Pt-7, and Pd/Pt-10 are 0.438, 0.801, 1.242, 1.661, and 2.521, respectively. With increasing sputtering time of Pt target, the relative

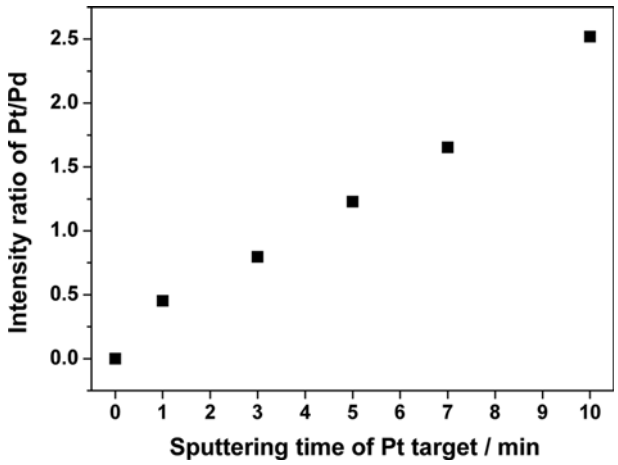

Fig. 4. Intensity ratios of Pt/Pd for the electrodes fabricated as a function of sputtering time of Pt target.

composition of Pt in the electrodes increases, thus resulting in an increased coverage of Pt on Pd electrodes (Fig. 4). This means that the Pt-deposited Pd electrodes, which might be well matched with a catalyst structure consisting of Pd core and Pt shell, can be designed via the two-step sputtering deposition process for catalysis of bi-layered electrodes.

Fig. 5 shows CVs of the Pd/Pt electrodes in Ar-saturated 0.1 M $HClO_4$ with a scan rate of 50 mV s^{-1} at room temperature. The characteristic peaks for the adsorption/desorption of hydrogen and pre-oxidation/reduction of oxygen on the electrode surfaces are clearly indicated. Typically, polycrystalline Pd and Pt electrodes exhibit particular oxygen reduction reaction (ORR) peaks at ~0.3 and ~0.6 V *vs.* Ag/AgCl, respectively, as follows: $O_2+4H^++4e^-\rightarrow 2H_2O$. The ORR peaks of the sputtered electrodes are shifted to a higher potential and can be also fitted by two peaks corresponding to oxygen reduction of Pd and Pt catalysts (Fig. 6(a)). The relative area ratios of the fitted ORR peaks are compared as shown in Fig. 6(b). With increasing sputtering time of Pt target, the area ratio corresponding to the ORR for the Pd electrode gradually decreases, representing in an increased coverage of Pt on Pd electrodes. In particular, pure Pd as a 2nd metal with similar binding energies of O and OH exhibits comparable activity to that of Pt in the ORR. It has been reported that Pt-Pd catalysts have excellent electrocatalytic activity due to the modified electronic structure of the electrodes in comparison with pure Pt. The modified electronic properties of the Pt-Pd catalysts might result from Pt containing negative charge and vacant valence d-orbital and Pd containing positive charge and fully occupied valence d-orbital. Recently, the Pt-Pd catalysts with Pt-rich composition have shown much higher oxygen reduction activity compared to pure Pt catalyst [12,13].

Methanol oxidation reactions (MORs) of the as-prepared electrodes in 0.1 M $HClO_4$+2.0 M CH_3OH with a scan rate of 50 mV s^{-1} are compared as shown in Fig. 7. Theoretically, methanol oxidation on Pt catalyst may proceed at 0.04 V vs. NHE as follows: $CH_3OH+H_2O\rightarrow CO_2+6H^++6e^-$. Therefore, the lower onset potential indicates a clear evidence of superior electrocatalytic activity for MOR. In the on-set potentials for MOR (Fig. 8(a)), the Pd/Pt-7 shows the lowest onset potential, i.e., an improved electrocatalytic activity. Also, at 0.5 V, the Pd/Pt-7 indicates the highest MOR current density as compared with other samples (Fig. 8(b)). The catalytic enhancement for MORs in the Pd/Pt-7 may be attributed to an electronic effect by an interaction between the core element and the shell element [14]. The shell is an important factor to control the electrocatalytic properties. The core-shell bimetallic catalysts might cause better suppression of adsorbed poisonous species during MOR, modifying electronic band structure to create better surface absorption [4,14]. As a result, Pd/Pt-7 having an optimized Pt coverage on the Pd electrode might be responsible for excellent electrocatalytic activity for MOR. Further practical works will be carried out using Pt/Pd nanoparticles for the MOR.

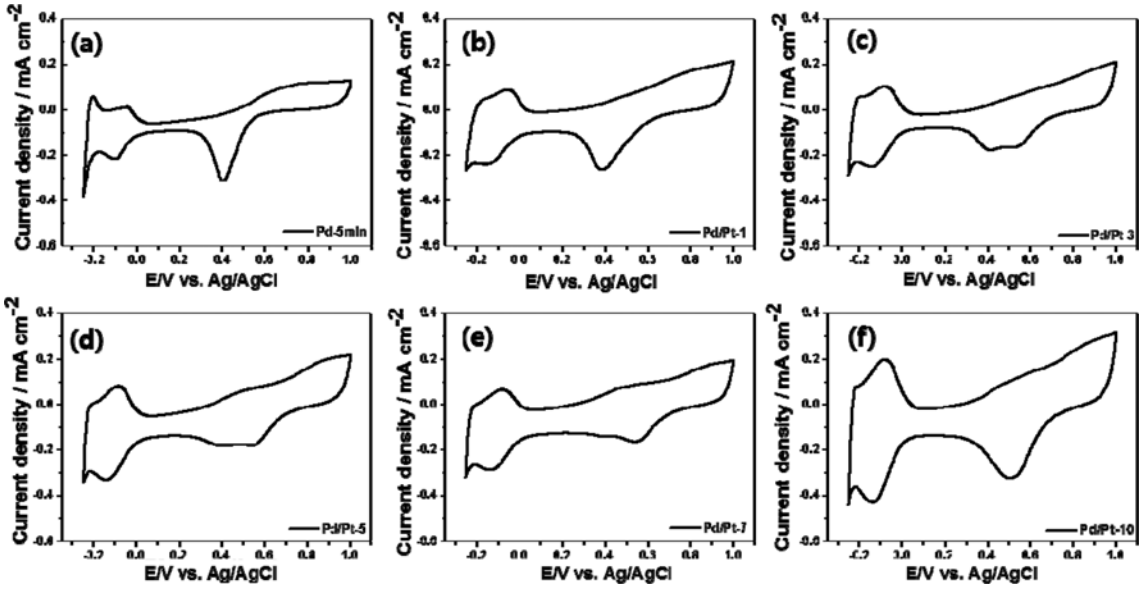

Fig. 5. CVs of the electrodes in Ar-saturated 0.1 M $HClO_4$ with a scan rate of 50 mV s^{-1} at room temperature: (a) Pd-only, (b) Pd/Pt-1, (c) Pd/Pt-3, (d) Pd/Pt-5, (e) Pd/Pt-7, and (f) Pd/Pt-10.

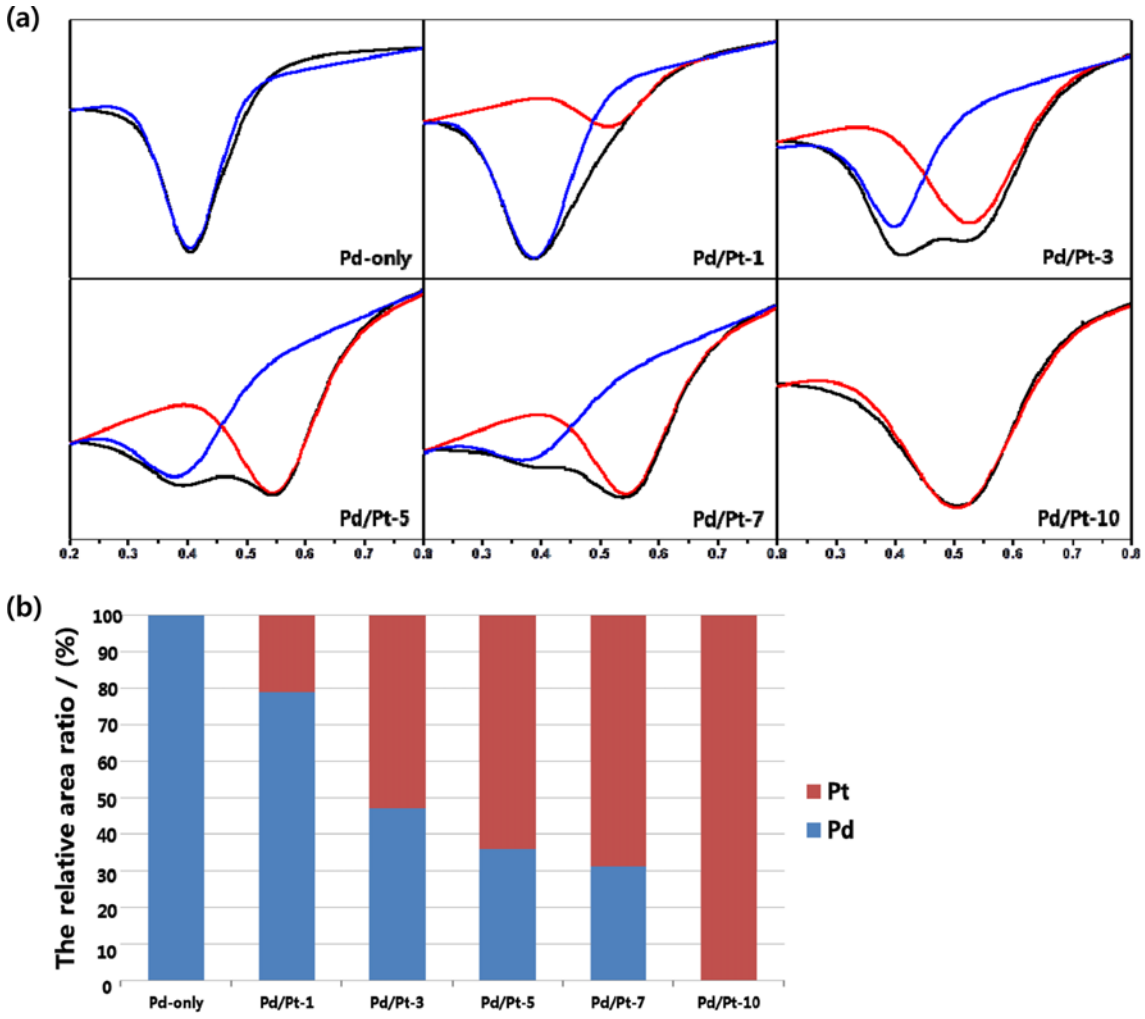

Fig. 6. (a) ORR peaks of the electrodes fitted by two peaks corresponding to oxygen reduction of Pd and Pt electrodes. (b) Relative area ratios of the fitted ORR peaks of the deposited electrodes.

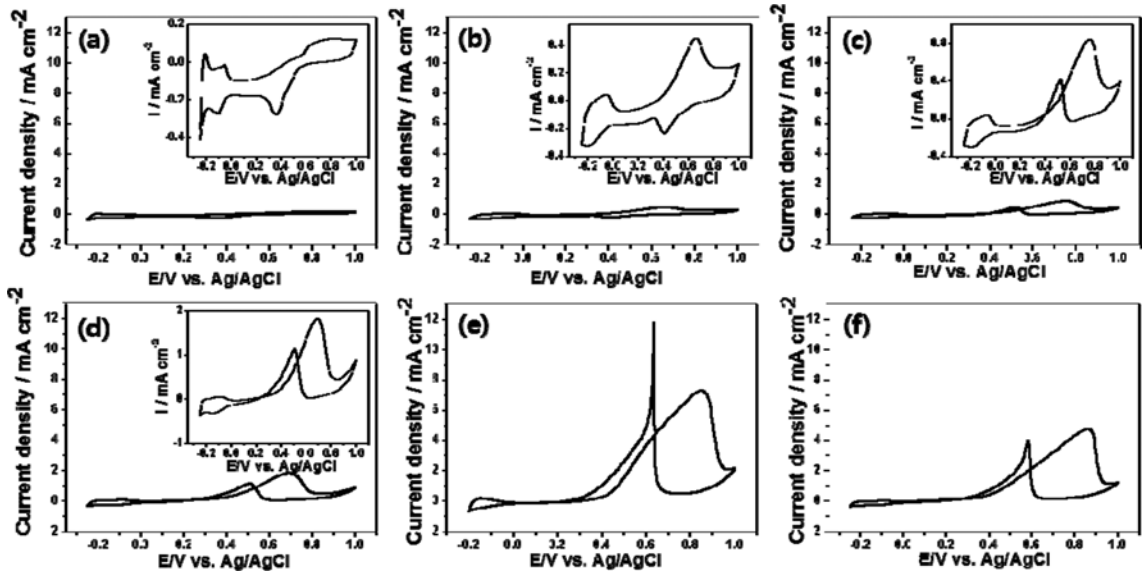

Fig. 7. CVs of the as-deposited electrodes for MOR in 0.1 M $HClO_4$+2.0 M CH_3OH with a scan rate of 50 mV s^{-1} at room temperature: (a) Pd-only, (b) Pd/Pt-1, (c) Pd/Pt-3, (d) Pd/Pt-5, (e) Pd/Pt-7, and (f) Pd/Pt-10. The insets of Fig. 7 (a)-(d) indicate the raw data.

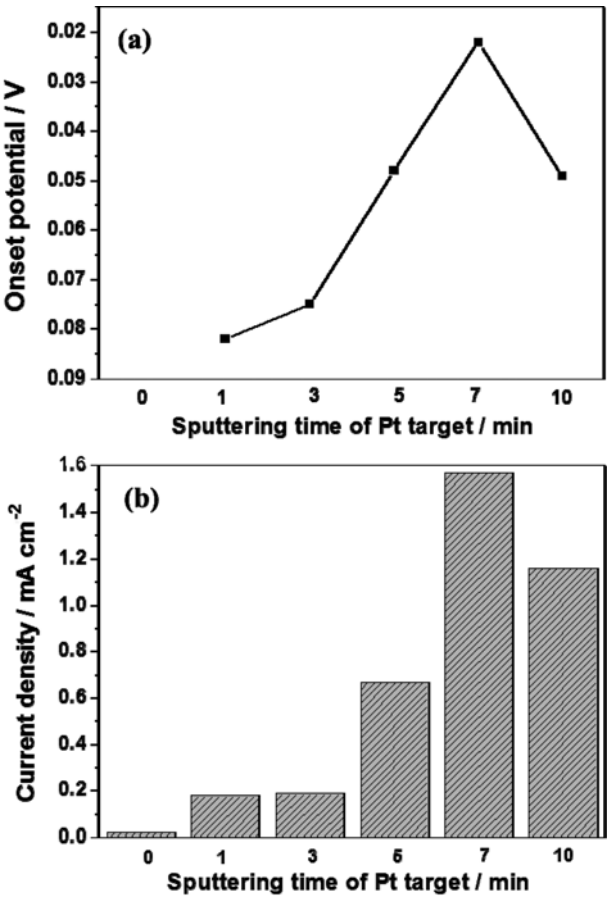

Fig. 8. (a) On-set potentials and (b) MOR current densities of the as-deposited electrodes fabricated as a function of sputtering time of Pt target.

CONCLUSIONS

We have fabricated Pt-deposited Pd nanostructure electrodes via a two-gun sputtering deposition process by separately operating Pd and Pt targets. As the deposition time of Pt target increases, the coverage of Pt on Pd electrodes can be elaborately controlled. The Pd/Pt-7 with an optimized Pt coverage shows an excellent electrocatalytic activity for MOR.

ACKNOWLEDGEMENTS

This research was supported by Basic Science Research Program through the National Research Foundation of Korea (NRF) funded by the Ministry of Education (NRF-2013R1A1A2012541).

REFERENCES

1. A. Caillard, C. Coutanceau, P. Brault, J. Mathias and J.-M. Léger, *J. Power Sources*, **162**, 66 (2006).
2. A. A. Dameron, T. S. Olson, S. T. Christensen, J. E. Leisch, K. E. Hurst, S. Pylypenko, J. B. Bult, D. S. Ginley, R. P. O'Hayre, H. N. Dinh and T. Gennett, *ACS Catal.*, **1**, 1307 (2011).
3. A. Dianat, N. Seriani, L. C. Ciacchi, W. Pompe, G. Cuniberti and M. Bobeth, *J. Phys. Chem. C*, **113**, 21097 (2009).
4. N. V. Long, T. D. Hien, T. Asaka, M. Ohtaki and M. Nogami, *Int. J. Hydrogen Energy*, **36**, 8478 (2011).
5. W. D. King, J. D. Corn, O. J. Murphy, D. L. Boxall, E. A. Kenik, K. C. Kwiatkowski, S. R. Stock and C. M. Lukehart, *J. Phys. Chem. B*, **107**, 5467 (2003).
6. K.-W. Park, J.-H. Choi, K.-S. Ahn and Y.-E. Sung, *J. Phys. Chem. B*, **108**, 5989 (2004).
7. H. Wang, M. Zhang, F. Cheng and C. Xu, *Int. J. Electrochem. Sci.*, **3**, 946 (2008).
8. I. S. Seo and S. W. Martin, *Inorg. Chem.*, **50**, 2143 (2011).
9. S. J. Hwang, S.-K. Kim, J.-G. Lee, S.-C. Lee, J. H. Jang, P. Kim, T.-H. Lim, Y.-E. Sung and S. J. Yoo, *J. Am. Chem. Soc.*, **134**, 19508 (2012).
10. K.-W. Park and Y.-E. Sung, *J. Phys. Chem. B*, **109**, 13585 (2005).
11. T.-W. Kim, S.-J. Park, L. E. Jones, M. F. Toney, K.-W. Park and Y.-E. Sung, *J. Phys. Chem. B*, **109**, 12845 (2005).
12. R. M. Anderson, L. Zhang, J. A. Loussaert, A. I. Frenkel, G. Henkelman and R. M. Crooks, *ACS Nano*, **7**, 9345 (2013).
13. J. Yang, W. Zhou, C. H. Cheng, J. Y. Lee and Z. Liu, *ACS Appl. Mater. Interfaces*, **2**, 119 (2010).
14. Y.-N. Wu, S.-J. Liao, Z.-X. Liang, L.-J. Yang and R.-F. Wang, *J. Power Sources*, **194**, 805 (2009).